Progress In Electromagnetics Research M, Vol. 105, 141–150, 2021

Breaking the Diffraction Limit Manifold Using Specially Designed Metamaterial Split Ring Resonator

Cherala Bindu[1, 2], Sikha K. Simon[1, 3], Anju Sebastian[1], Panattil V. Aswathi[1], Dona Joseph[1], Jolly Andrews[1], and Vallikkavumkal P. Joseph[1, *]

Abstract—A novel and efficient method to overcome the barriers of conventional diffraction limit using a specially designed metamaterial Split Ring Resonator (SRR) structure as an imaging sensor at microwave frequency is proposed. The topology of the proposed sensor is ingeniously designed to identify imaging objects having dimensions much less than the interacting wavelength λ. The split gap field region of the conventional SRR, used as the sensing region of the imaging sensor, is modified for enhancing the resolution capacity, by slightly raising the split region of the outer ring structure perpendicular to the plane of the resonator (Projected Split Ring Resonator — PSRR) which will reduce the area of the sensing region of the SRR probe considerably. The isolation of the structural parts of the SRR other than projected split region helps in using the localized evanescent field at the split region of the PSRR for imaging of minute objects having dimension ranges up to 0.0001λ by precisely choosing the split gap. The required projection height of the split region and the possible resolution limits of the PSRR sensor probe are evaluated by simulation. Experimental 2-dimensional sub-wavelength images obtained for various dielectric objects using a typical PSRR test probe having resolution capability up to 0.01λ are also presented.

1. INTRODUCTION

Microwave based imaging techniques have been used for various sensor applications due to their non-destructive and non-invasive nature. Different types of metamaterial structural units and surfaces have been widely proposed recently for various modes of sensors [1–6]. Near field microwave probes can confine evanescent fields to regions having dimensions much smaller than operating wavelength, and hence they are able to resolve sub-wavelength features and thereby provide a resolution much higher than the classical Abbe limit [7, 8]. Earlier microwave near-field techniques mainly focused on a topology of microstrip line resonator terminated with a sharpened tip or a small loop and were reported to achieve a better resolution in dielectrics [9–11]. With sophisticated experimental setup, they were able to map material non-uniformities by carefully designed conductivity mapping technique [12]. Later, the possibility of making a perfect lens using metamaterial structures and thereby achieving a resolution higher than classical diffraction limit was theoretically proposed in the pioneering work of Pendry [13]. In that work, the concept of a negative refractive index material capable of completely restoring both propagating and evanescent waves in phase and amplitude resulting in the recovery of sub-wavelength features leading to a perfect imaging of the sample was presented. Microwave near-field probe made of single rectangular Split Ring Resonator (SRR), and an electrically small rectangular loop was designed by Ren et al. which provided a resolution of $\lambda/74$ based on sub-surface detection technique [8]. For the purpose of obtaining super resolution imaging using metamaterial structures, specially designed

Received 12 September 2021, Accepted 22 October 2021, Scheduled 31 October 2021

* Corresponding author: Vallikkavumkal Paily Joseph (vpj@christcollegeijk.edu.in).

[1] Christ College (Autonomous), Irinjalakuda, University of Calicut, Kerala, India. [2] Govt. Women's Polytechnic College, Nedupuzha, Thrissur, Kerala, India. [3] St. Thomas' College (Autonomous), Thrissur, University of Calicut, Kerala, India.

topologies have to be introduced, since the conventional SRRs can provide the imaging resolutions of the order of $\lambda/15$ only [14]. A modification in this direction is reported as Folded Split Ring Resonator (FSRR) which enabled reducing the sensing area of conventional SRR whereby a superior performance in resolution around $\lambda/30$ was achieved [15]. Later a specially designed SRR with enhanced imaging capability is proposed for sensing applications which is found to achieve a resolution of the order of $\lambda/100$ [16].

In this paper, the sub-wavelength imaging of the order of $\lambda/10000$ is reported for the first time using simulation method by making use of an SRR having precisely designed split topology named Projected Split Ring Resonator (PSRR), which uses the evanescent field near a narrow split region for sensing purpose. For further enhancing the resolution limits, an analysis of topological modifications required is included. The experimental results obtained for a typical imaging PSRR probe for a 2-D object with dimensions of the order of $\lambda/100$ are also presented.

2. DESIGN AND SIMULATION

The resonance frequency of an SRR is evaluated in terms of its intrinsic capacitive and inductive terms using the basic equation

$$f = \frac{1}{2\pi\sqrt{LC}} \tag{1}$$

where L is the effective inductance, and C is the effective capacitance. For analysing the resonance frequency of the SRR, various methodologies including certain analytical models are proposed in literature [13, 17–20].

The schematic diagram of the test probe used for high resolution imaging is shown in Fig. 1(a). Unlike conventional SRR, this novel topological design is fabricated by slightly raising a small length l of the split region of the outer ring to a height h by which the localised evanescent field near the split region is isolated from the field regions of the remaining portions of the SRR. The advantage of raising the split region is that it considerably reduces the probing area in comparison to the actual size of the SRR resulting in a drastic enhancement of the resolution capability. It was established in an earlier work [17] that the extent to which the evanescent field is present on the top and bottom sides of the SRR from its plane is only up to a distance equal to $c + d/2$, where c is the width of each ring, and d is the spacing between rings of the resonator structure (Fig. 1(a)). In view of this, the projection height h of the split region, which acts as the scanning region of the SRR probe used for the present work is optimised to a height equal to or slightly greater than $c + d/2$, in order to isolate the field effect of the regions of the SRR probe other than the projected split region on the scanning object. Initially, the field distribution around a conventional SRR is examined using simulation by carefully analysing the interaction of a dielectric slab with the near-field energy of the SRR probe using high frequency simulation software. For this, a conventional SRR of inner radius $r = 3.15\,\text{mm}$, width of ring

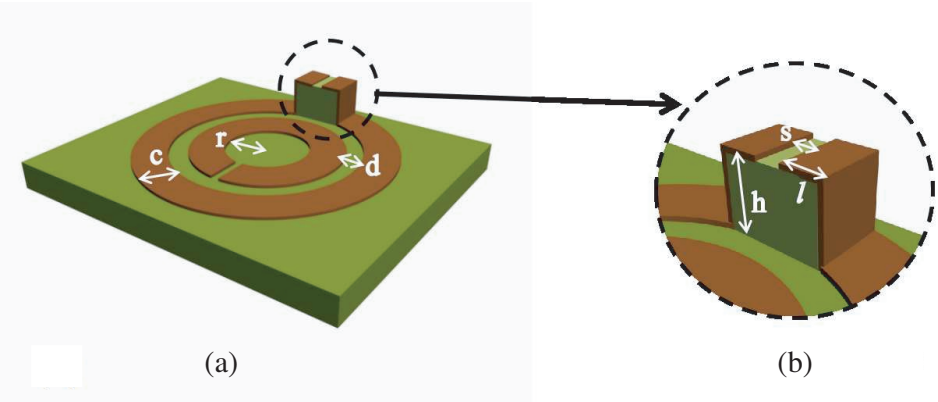

Figure 1. Schematic diagram of the PSRR (a) along with a magnified view of projected split region, (b) showing its structural dimensions — inner radius (r), width of the ring (c), spacing between rings (d), height of projection (h), split width (s) and length of projected part (l).

$c = 0.7$ mm, spacing between rings $d = 0.8$ mm, and split width $s = 0.5$ mm is considered. A dielectric slab of area 10 mm × 10 mm, which is sufficient to cover the surface area of the SRR with thickness 2 mm is placed over one side of the SRR. This dielectric slab is slightly moved away from the SRR plane, and the shift in resonance frequency is analysed for different spacings (x) between the SRR plane and the dielectric slab by simulations. It is observed that as the spacing x increases, the resonance frequency increases gradually as depicted in Fig. 2(a) up to a distance around $c + d/2$ whereupon its value remains constant. A schematic arrangement of the probe-dielectric setup is pictured in Fig. 2(b).

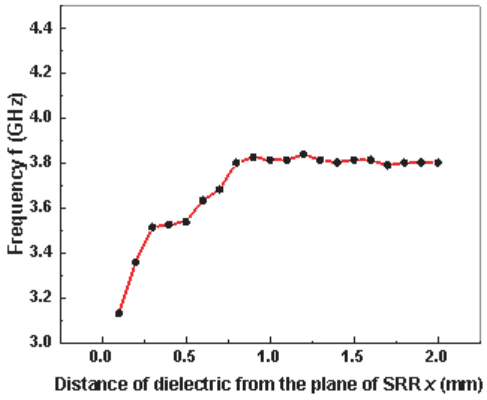

(a)

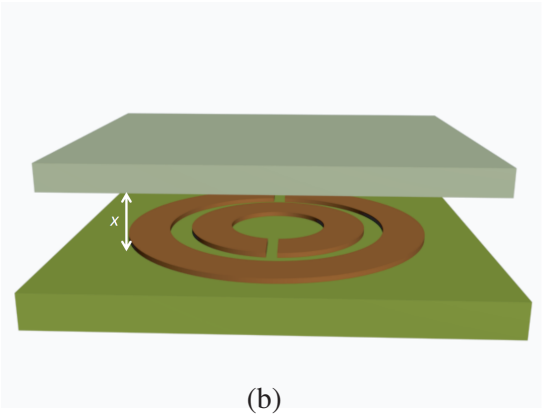

(b)

Figure 2. (a) Plot showing the variation of resonant frequency with distance x of dielectric slab (area 10 mm × 10 mm and thickness 2 mm) from the plane of SRR. (b) Schematic arrangement of the probe — dielectric setup.

For the present probe, this constant value obtained in simulation is around 1.1 mm, which is exactly equal to the predicted distance $c + d/2$, and for any further increase in spacing x, the change in resonance frequency observed is found to be insignificant. As the next step, to evaluate the high resolution capability of the proposed new variant of SRR having projected split region (PSRR), its interaction with a thin rectangular dielectric rod is carried out for a precisely selected operating frequency f_{op}. For this the conventional SRR structure used for analysing the near field distribution is modified to a PSRR imaging probe by raising the split region as shown in Fig. 1(b) to a height of 1.1 mm, which is equal to $c + d/2$ for the present case, thereby achieving the isolation of the sensing region from the field effect of the remaining portion of the SRR. The value of l, the length of each projected part of the strip, is taken as 0.8 mm, and the split width s is kept same as 0.5 mm.

The operating frequency f_{op} of the test probe for imaging sub-wavelength objects is selected from the resonance absorption curve of the PSRR probe. The simulated transmission curve (S_{21}) of the PSRR imaging test probe is plotted in Fig. 3 which shows a resonant absorption f_0 around 3.6 GHz. If f_{op} selected is slightly greater than f_0, somewhere on the raising portion AB of the resonance curve a, any decrease occurring to the resonant frequency due to the presence of a dielectric material (imaging object) near the projected split region of the PSRR test probe causes an increase in transmitted power level as demonstrated using curve b in Fig. 3. When some dielectric material capable of sensing by the projected sensing region of the PSRR test probe is placed near the split region, the effective capacitance of the resonator increases which causes a lowering of the resonance frequency. If the operating frequency selected is around 3.7 GHz, the power level corresponding to this frequency P_1 increases to P_2 when the dielectric object moves towards the sensing region as the resonance curve shifts to lower frequency side. If the size or dimensions of the dielectric are very small such that its presence is not sensed by the probe, such dimensions of the object may be treated as smaller than the resolution limit of the probe. For checking the resolvable size of the test probe, the simulation procedure as detailed below is followed.

A rigid thin polyester sheet of thickness 0.1 mm and dielectric constant $\epsilon_r = 3.5$ is set in the form of a platform above the PSRR probe parallel to the plane as shown in Fig. 4 with the top of the split

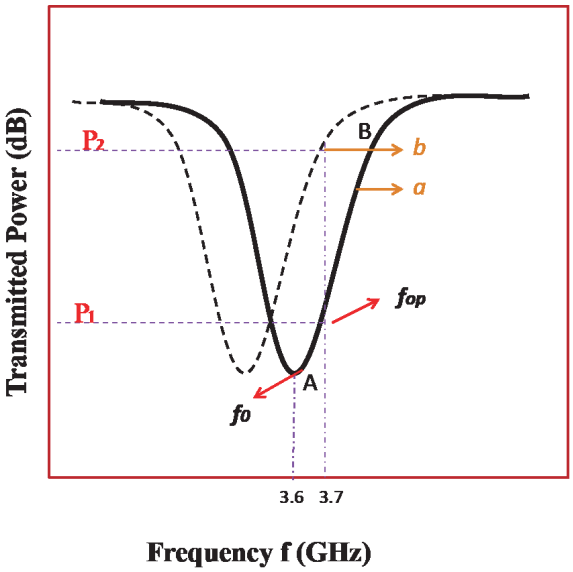

Figure 3. Simulated S_{21} characteristic curve of the PSRR test probe alone *(a)* and test probe with a thin rectangular dielectric rod placed on the top of its split region *(b)*.

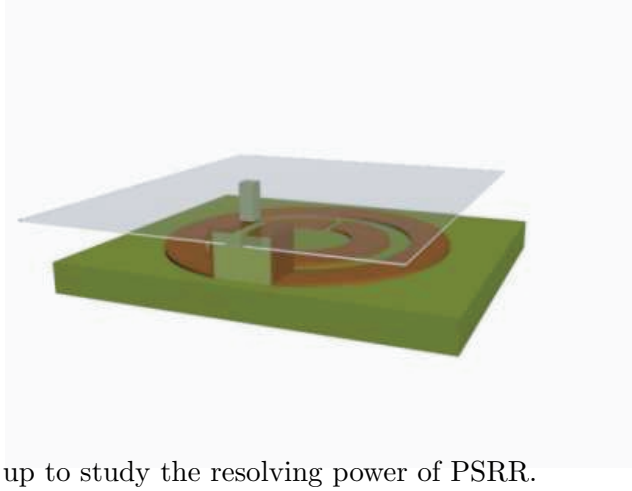

Figure 4. Simulation set up to study the resolving power of PSRR.

region almost touching (0.1 mm gap) it. The dielectric strip, which serves as the scanning object is placed on the top of the platform as shown in the figure. This dielectric strip of width 1 mm (along the direction parallel to the split gap) and breadth 1 mm (along the direction perpendicular to split gap) with a height of 3 mm having dielectric constant $\epsilon_r = 4.4$ is moved over the platform horizontally (along the direction of the split as shown by the dotted line of the inset picture of Fig. 5), and the measured transmitted power corresponding to the excitation frequency at f_{op} is plotted as curve 1 in Fig. 5.

The power received when the dielectric strip is near the sensing split region of the PSRR probe is high which clearly verifies the sensing capability of the probe for the specified dimension of the scanning object. In comparison to the wavelength λ (102 mm) corresponding to the operating frequency, the size of the imaged object (1 mm) of the dielectric strip is around $\lambda/100$ (resolving power). The power level obtained for another dielectric rod with width and breadth 0.1 mm using the same PSRR structure having the same split gap 0.5 mm is depicted in curve 2 of Fig. 5, which verifies the enhanced resolving capacity of the probe for a dimension of $\lambda/1000$. Further reduction in size of the rod produces only very small changes in the received power level as the dielectric is moved towards the proximity of the split region of the PSRR. Hence, for the proposed PSRR structure with specified split gap 0.5 mm, the maximum resolution power of object is around $\lambda/1000$.

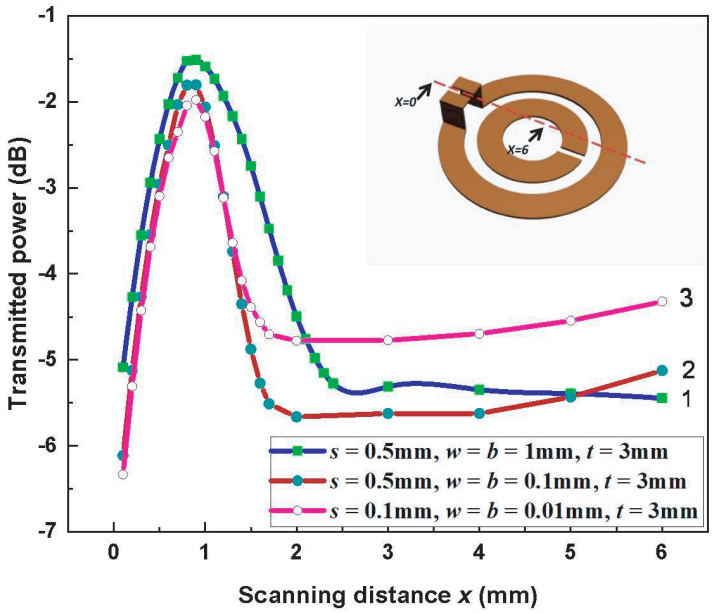

Figure 5. Transmitted power of the PSRR probe with scanning distance X for different dielectric strips of width w, breadth b and height t for probes having split width s. The inset shows a schematic representation of a PSRR probe showing the direction of movement (dashed line) of the dielectric strip.

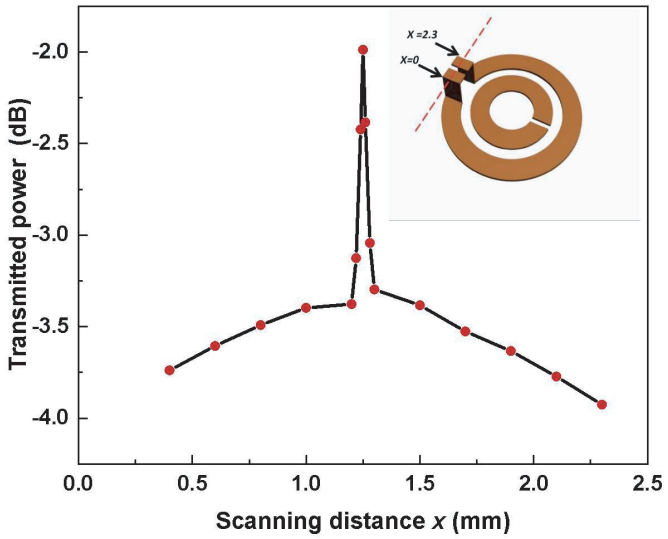

Figure 6. Transmitted power of the PSRR probe (split gap 0.1 mm) with scanning distance X for a dielectric strip of width and breadth 0.01 mm. The inset shows a schematic representation of a PSRR probe showing the direction of movement (dashed line) of the dielectric strip parallel to the split gap.

These simulation studies using the interaction of the near field at the split of the PSRR with the dielectric rod have drawn out a clear relation between the resolving power and the split width of the projected part of the PSRR. For a further enhancement of resolving power, a decrease in split gap is suggested. The simulation results obtained using a PSRR test probe with a reduced split gap of 0.1 mm,

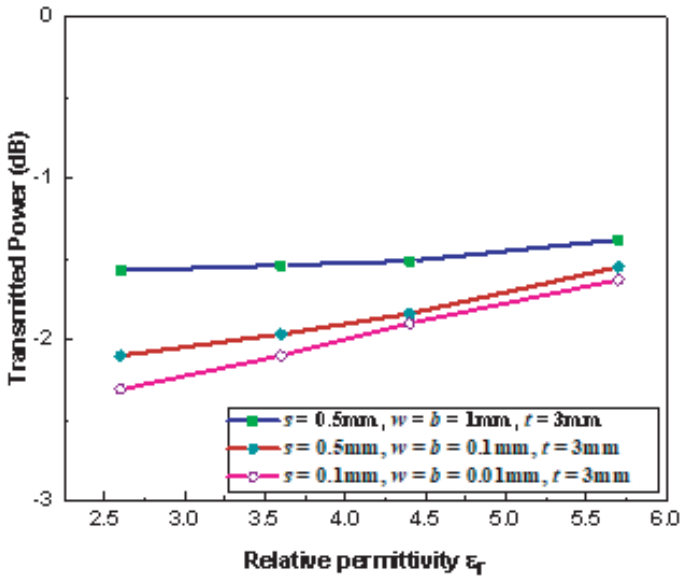

Figure 7. Transmitted power of the PSRR probe for different permittivity values of various dielectric samples of width w, breadth b and height t for probes having split width s.

keeping all other dimensions constant are pictured in curve 3 of Fig. 5. The width and breadth of the dielectric used are 0.01 mm, and it is very clearly identified by the sensor. In terms of the excitation wavelength of the PSRR probe, the identified width of the rod is around $\lambda/10000$. It is thus verified that by decreasing the split gap of the sensor probe, the resolving power can be enhanced considerably which helps to resolve very thin objects in terms of the sub-wavelength scale.

For further confirmation, simulations are performed when the object is moved parallel to the split gap with the same scanning probe and object (strip width and breadth = 0.01 mm each and split gap = 0.1 mm). Fig. 6 shows the corresponding transmitted power which clearly depicts the accurate detection of the object near the split gap region with the same enhanced resolution of $\lambda/10000$. In order to study the power level corresponding to samples of different dielectric constants, simulations are carried out with dielectrics of permittivity 2.6, 3.6, 4.4, and 5.7 for probes and samples mentioned in Fig. 5. The simulated result is given as Fig. 7. It is observed that for samples of low dielectric constant, the resonant frequency increases, and consequently the corresponding power level decreases. For materials with increased dielectric constant values, the inverse result is observed.

3. EXPERIMENTAL CONFIRMATION

The sub-wavelength imaging capability of the proposed novel split ring resonator with projected split region is verified experimentally using a PSRR test probe having resolution limit around $\lambda/100$. 2-dimensional sub-wavelength images of some small collections of tiny dielectric objects like sand and glass pieces are obtained using a setup consisting of a PSRR probe and a precision X-Y scanner. A photograph of the experimental setup is given in Fig. 8.

The PSRR is set between the transmitting and receiving probes of a Vector Network Analyser (VNA). It is then attached to the movable unit of a microcontroller based precision X-Y scanner so as to make the PSRR probe capable of sensitive movement in the X and Y directions with a precision of 0.1 mm. To fabricate the PSRR, a conventional SRR is initially developed using a thin copper film of thickness 20 µm by chemical etching method, and it is carefully fixed on an FR4 dielectric substrate ($\epsilon_r = 3.6$). During this fabrication process, maximum care is taken for precisely raising the outer split gap region to a height h above the plane of the SRR as depicted in Fig. 1. For this, the copper film at the outer split gap region is peeled and folded vertically using specially designed forceps. A dielectric

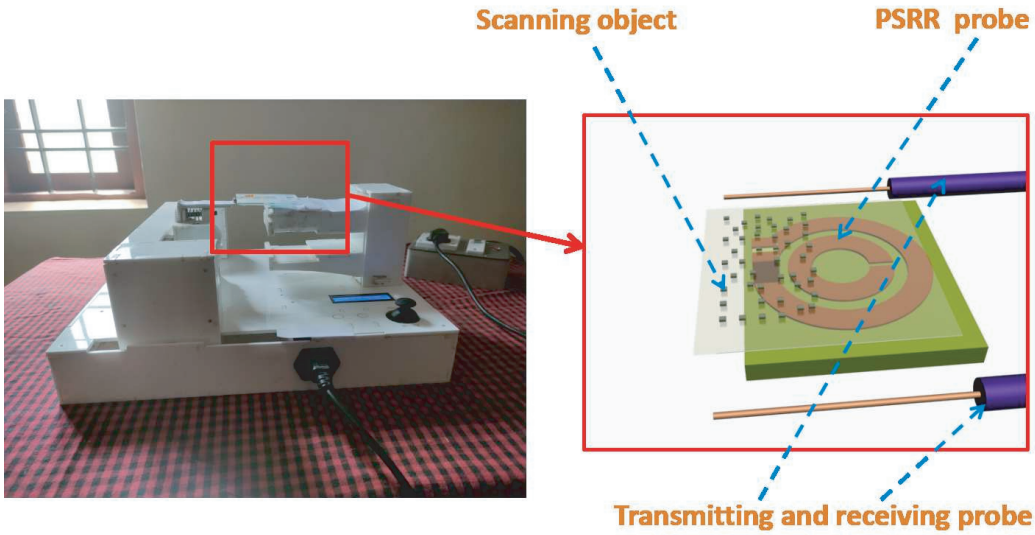

Figure 8. (a) Experimental setup showing PSRR probe along with the scanning objects placed on the X-Y scanner. (b) Schematic representation of the probe and scanning objects (sand particles) placed on rigid platform.

strip is then fixed between the folded vertical strips. Another metallic film of the same width is carefully placed on the top of the dielectric piece, and the edges are soldered to the vertical ends. Finally, the required split is made on the projected part using a precision cutter. The structural dimensions of the PSRR structure are inner radius $r = 2\,\text{mm}$, ring width $c = 0.75\,\text{mm}$, spacing between the rings $d = 0.5\,\text{mm}$, projection height $h = 1.1\,\text{mm}$, length of the projected part $l = 0.8\,\text{mm}$, and split gap $s = 0.5\,\text{mm}$.

A rigid sheet made of polyester of thickness 0.1 mm and dielectric constant 2.4 is set just above the PSRR test probe in the form of a platform. The experimental transmission curve of the PSRR imaging test probe obtained is plotted in Fig. 9. The resonant frequency of the probe is around 4.68 GHz. The operating frequency is selected as 4.69 GHz which is on the linear portion of the raising part of the

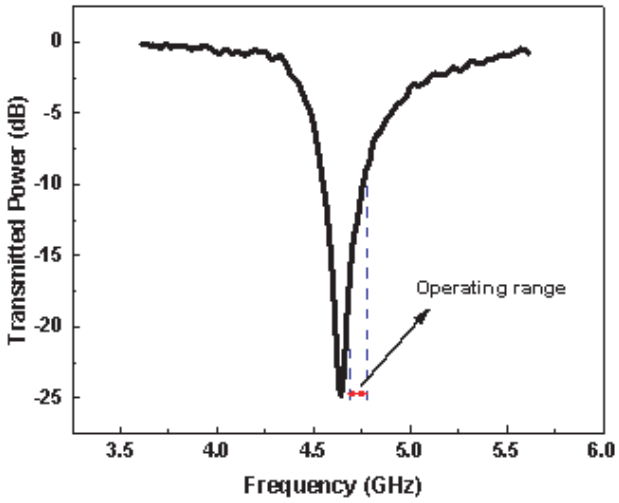

Figure 9. Experimental resonance curve of the PSRR test probe showing the operating range.

resonance curve on the right side as shown in figure.

The scanning object under study is placed on the platform as depicted in Fig. 8, and the PSRR is excited at the operating frequency. The sub-wavelength imaging characteristics of the PSRR test probe were analysed using three dielectric patterns (imaging objects) made of sand particles and glass chips. The first scanning object is a pattern consisting of three particles of silica sand of irregular shape having average larger dimension 6 mm with separation less than 1 mm between the closely spaced particles. Figs. 10(a) & (b) give the photograph of the pattern, and its 2-D sub-wavelength image obtained using the PSRR imaging probe. Spacing less than 1 mm (0.8 mm) is well resolved in the image, which is around $\lambda/80$ corresponding to the operating frequency of 4.69 GHz. Since the sand particles are irregular in shape, the resolved image clearly depicts the area of contact of the particles with the platform which may appear to have slight deviation of the actual photograph when being viewed from above.

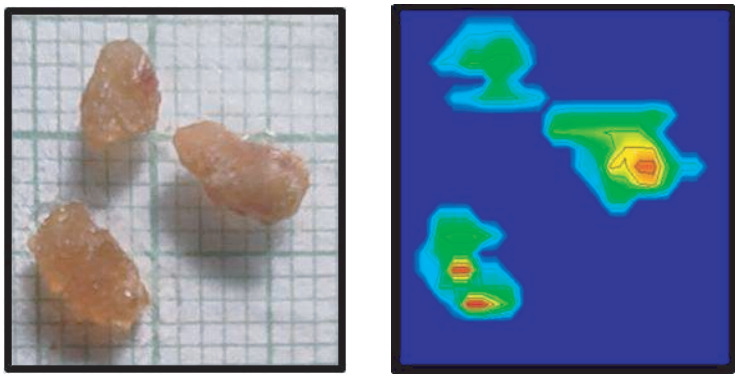

(a) (b)

Figure 10. (a) Photograph of dielectric pattern of sand particles and (b) the experimental 2-D sub-wavelength image obtained using the PSRR probe.

A photograph of the second dielectric pattern used for imaging is given in Fig. 11(a) which consists of two round-shaped and one triangle-shaped plane glass pieces of dielectric constant 6.3. The scanned image obtained is given in Fig. 11(b). Figs. 12(a) & (b) are the photograph and sub-wavelength image obtained for another dielectric pattern made of glass and perspex chips. The rectangle-shaped part imaged in red colour is of glass with dielectric constant 6.3, and the other irregular shape pieces are of perspex with dielectric constant 2.4. These images depict their sub-wavelength imaging features along with some insight related to the relative magnitude of the dielectric constant of the imaging

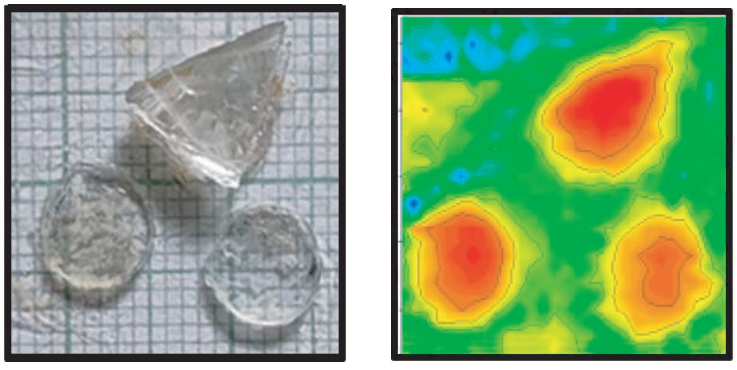

(a) (b)

Figure 11. (a) Photograph of dielectric pattern of glass pieces and (b) the experimental 2-D sub-wavelength image obtained using PSRR probe.

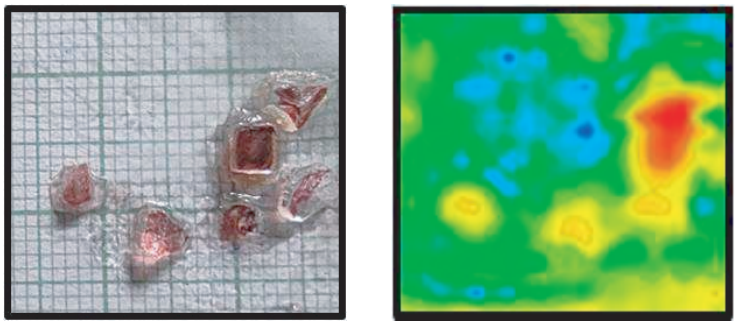

(a) (b)

Figure 12. (a) Photograph of dielectric pattern of glass and perspex chips and (b) the experimental 2-D sub-wavelength image obtained using PSRR probe.

objects. While the experiment is performed, extreme care is taken for avoiding any possible noise factor. The probe is fixed in a rigid manner, and the possibility of it getting vibrated or disturbed is almost eliminated and thereby the data obtained are ensured to be free from any significant noise effects.

4. CONCLUSIONS

A novel Projected Split Ring Resonator (PSRR) structure specially designed for sensing applications with enhanced imaging capability is proposed. This is achieved by carefully engineering the outer split gap region of the conventional SRR to an optimum height which acts as a high resolution sensing region whereby the possibility of breaking the diffraction limit around a range of one in ten-thousandth of the wavelength used can be realized. Further enhancement of the resolving power can be achieved by precisely designing the split gap and topology of the split region. The selected simulation results are verified experimentally using 2-D sub-wavelength imaging of specific samples. By analysing the relation between split gap and resolving power and by employing precise computer aided designs, further improvements in the resolution limits of the test probe can be achieved. This novel PSRR structure and the newly proposed high resolution imaging technique may find wide range of applications in non-destructive sensing devices which may be particularly useful in biomedical fields.

ACKNOWLEDGMENT

Aswathi P. V. gratefully acknowledges Kerala State Council for Science, Technology and Environment (KSCSTE), Kerala for the financial support under KSCSTE research fellowship.

REFERENCES

1. Simon, S. K., S. P. Chakyar, A. Sebastian, J. Jose, J. Andrews, and V. P. Joseph, "Broadside coupled split ring resonator as a sensitive tunable sensor for efficient detection of mechanical vibrations," *Sensing and Imaging*, Vol. 20, No. 17, 1–11, 2019.
2. Umadevi, K. S., S. P. Chakyar, S. K. Simon, J. Andrews, and V. P. Joseph, "Split ring resonators made of conducting wires for performance enhancement," *EPL*, Vol. 118, No. 24002, 1–5, 2017.
3. Sebastian, A., S. K. Simon, S. P. Chakyar, J. Jose, V. P. Joseph, and J. Andrews, "Broadside coupled split ring resonator metamaterial structure for sensitive measurement of liquid concentrations," *AIP Confer. Proceedings*, Vol. 2082, No. 07002, 1–4, 2019.
4. Thomas, H., S. P. Chakyar, S. K. Simon, J. Andrews, and V. P. Joseph, "Transmission line coupled split ring resonator as dielectric thickness sensor," *AIP Confer. Proceedings*, Vol. 1849, No. 020003, 1–6, 2017.

5. Valagiannopoulos, C. A., "High selectivity and controllability of a parallel plate component with a filled rectangular ridge," *Progress In Electromagnetics Research*, Vol. 119, 497–511, 2011.
6. Lee, Y., S. J. Kim, H. Park, and B. Lee, "Metamaterials and metasurfaces for sensor applications," *Sensors*, Vol. 17, No. 1726, 1–28, 2017.
7. Matbouly, H. El., "Review on microwave metamaterial structures for near-field imaging," *Microwave Systems and Applications*, 359–372, 2017.
8. Ren, Z., M. S. Boybay, and O. M. Ramahi, "Near field probes for subsurface detection using split ring resonator," *IEEE Trans.Microwave Theory Tech.*, Vol. 59, No. 2, 1064–1076, 2011.
9. Azar, M. T., N. S. Shoemaker, and S. Harris, "Non-destructive characterization of materials by evanescent microwaves," *Meas. Sci. Technol.*, Vol. 4, No. 10, 583–590, 1993.
10. Azar, M. T., D. P. Su, A. Pohar, S. R. Leclair, and G. Ponchak, "0.4 μm spatial resolution with 1 GHz ($\lambda = 30$ cm) evanescent microwave probe," *Rev. Sci. Instrum.*, Vol. 7, No. 3, 1725–1729, 1999.
11. Azar, M. T., P. S. Pathak, G. Ponchak, and S. Leclair, "Nondestructive super resolution imaging of defects and non uniformities in metals, semiconductors, dielectrics, composites, and plants using evanescent microwaves," *Rev. Sci. Instrum.*, Vol. 70, No. 6, 2783–2792, 1999.
12. Azar, M. T., J. L. Katz, and S. R. Leclair, "Evanescent microwaves: A novel super-resolution noncontact nondestructive imaging technique for biological applications," *IEEE Trans. Instrum. Meas.*, Vol. 48, No. 6, 1111–1116, 1999.
13. Pendry, J. B., "Negative refraction makes a perfect lens," *Phys. Rev. Lett.*, Vol. 85, No. 18, 3966–3969, 2000.
14. Chen, T., S. Li, and H. Sun, "Metamaterial application in sensing," *Sensors*, 2742–2765, 2012.
15. Bindu, C., S. P. Chakyar, A. Sebastian, S. K. Simon, J. Jose, N. Paul, K. S. Umadevi, J. Kizhakooden, J. Andrews, and V. P. Joseph, "Enhancing the resolution in imaging using folded metamaterial split ring resonator structure at microwave frequencies," *AIP Confer. Proceedings*, Vol. 2162, No. 020067, 1–5, 2019.
16. Bindu, C., S. P. Chakyar, A. Sebastian, J. Andrews, and V. P. Joseph, "Specially designed metamaterial split ring resonator for high resolution imaging at Microwave frequencies," *IEEE Metamaterial Conference Proceedings*, x450–x452, 2019.
17. Chakyar, S. P., S. K. Simon, C. Bindu, J. Andrews, and V. P. Joseph, "Complex permittivity Measurement using metamaterial split ring resonators," *Journal of Applied Physics*, Vol. 121, No. 054101, 1–6, 2017.
18. Valagiannopoulos, C. A., "Electromagnetic propagation into parallel plate waveguide in the presence of a skew metallic surface," *Electromagnetics*, Vol. 31, No. 8, 593–605, 2011.
19. Sydoruk, O., E. Tatartschuk, E. Shamonina, and L. Solymar, "Analytical formulation for the resonant frequency of split rings," *AIP Jornal Applied*, Vol. 105, No. 014903, 1–4, 2009.
20. Tagay, Z. and C. A. Valagiannopoulos, "Highly selective transmission and absorption from metasurfaces of periodically corrugated cylindrical particles," *Phy. Re.*, Vol. 98, No. 115306, 1–10, 2018.